SIAM J. CONTROL OPTIM.
Vol. 50, No. 1, pp. 243–265

AN EULERIAN APPROACH TO THE ANALYSIS OF KRAUSE'S CONSENSUS MODELS*

C. CANUTO†, F. FAGNANI†, AND P. TILLI†

Abstract. In this paper we analyze a class of multiagent consensus dynamical systems inspired by Krause's original model. As in Krause's model, the basic assumption is the so-called bounded confidence: two agents can influence each other only when their state values are below a given distance threshold R. We study the system under an Eulerian point of view considering (possibly continuous) probability distributions of agents, and we present original convergence results. The limit distribution is always necessarily a convex combination of delta functions at least R far apart from each other: in other terms these models are locally aggregating. The Eulerian perspective provides the natural framework for designing a numerical algorithm, by which we obtain several simulations in 1 and 2 dimensions.

Key words. multiagent systems, bounded confidence, Krause's model, Lyapunov stability, push-forward, Eulerian approach

AMS subject classifications. 39A30, 91C20, 93D20

DOI. 10.1137/100793177

1. Introduction.

Recently, a large amount of literature from control theory and information engineering has focused on the analysis of multiagent consensus models. They consist of a set of agents V indexing a family of coupled dynamical systems: for each $j \in V$ we have a dynamic evolution $x_j(t) \in \mathbb{R}^q$, for $t \in \mathbb{Z}$, governed by the law

$$x_j(t+1) = x_j(t) + \sum_{k \in V} P_{jk}(x_k(t) - x_j(t)). \tag{1}$$

P is, normally, a substochastic matrix so that the right-hand side can be read as a convex combination of all the systems states $x_k(t)$. In P, structural properties of the system are coded; for instance, the pairs (j,k) such that $P_{jk} \neq 0$ naturally describe a sort of communication network topology among the agents saying which agents are affecting whom. P may be constant or depend on time, or it can be deterministic or random. In a wide range of situations it has been shown that, for any possible initial condition, all dynamics $x_j(t)$ converge to the same value, namely to a so-called consensus value. Scientific fields where such models have appeared include load balancing in computer networks, distributed inferential algorithms for sensor networks, multiagent robots, and opinion dynamics models. For details, see [4, 6, 7, 10, 11, 16, 15, 17, 18, 21] and the references therein.

The case analyzed in this paper is that when the matrix P explicitly depends on the states of the agents, more precisely, when $P_{jk} = P_{jk}(x_k(t) - x_j(t))$. This is a particularly natural choice in multiagent robots models, where the possibility of communicating attenuates (and possibly vanishes) as distance grow [11], as well as in opinion dynamics models, where it is generally assumed that the willingness to change opinion follows a similar rule [16] (bounded confidence models). The most

*Received by the editors April 22, 2010; accepted for publication (in revised form) October 20, 2011; published electronically January 19, 2012. A preliminary short version of this paper has appeared in [5].

http://www.siam.org/journals/sicon/50-1/79317.html

†Dipartimento di Matematica, Politecnico di Torino, Corso D. Abruzzi, 24, 10129 Torino, Italy (ccanuto@calvino.polito.it, fabio.fagnani@polito.it, paolo.tilli@polito.it).

famous model of this type is Krause's model [12], where communication drops down beyond a threshold R:

$$P_{jk} = \begin{cases} N_j(t)^{-1} & \text{if } |x_j(t) - x_k(t)| \le R, \\ 0 & \text{otherwise,} \end{cases} \tag{2}$$

where $|\cdot|$ is the Euclidean norm in $\mathbb{R}^q$ and $N_j(t)$ is the number of agents $k \in V$ within distance R from $x_j(t)$ at time t. These state-dependent models are particularly difficult to analyze, because the dynamical system (1) becomes nonlinear. Moreover, in models like Krause's, where P_{jk} is 0 if the two positions (opinions) $x_j(t)$ and $x_k(t)$ are sufficiently far apart, there is the additional difficulty that the graph of possible connections among the agents changes with time, and can possibly disconnect.

Some papers have treated these models by considering the time variations in the matrix P as an exogenous signal [11], decoupled from the dynamics, and they show that when making suitable assumptions on the long-range connections of the time-varying communication graph, convergence to a consensus value is achieved. In [14] a first general convergence result for the coupled model is presented: if the following two conditions are satisfied:

- there is a threshold $\delta > 0$ such that $P_{jk} \neq 0$ yields $P_{jk} \ge \delta$,
- $P_{jk} > 0$ implies $P_{kj} > 0$,

then (1) always converges to a limit configuration $\{x_k(\infty)\}$. In the case of Krause's model, the limit configuration is characterized by the property that, for any two agents i and j, $x_i(\infty)$ and $x_j(\infty)$ are either equal or their distance is larger than R. If we assume that the initial positions $x_i(0)$ all stay in a hypercube $K = [-L, L]^q$, the set of limit positions $\Omega = \{x_i(\infty)\}$ will be a subset of K, in particular, $|\Omega| = O(2L/R)^q$ (independently of the number of agents). The exact cardinality of Ω of course depends on the initial positions. Simulations (in the case $q = 1$) presented in [2] seem to indicate that for a large number of agents uniformly distributed on the interval, $|\Omega| \approx L/R$ (the limit positions are about $2R$ apart). The authors in [2] propose some stability argument considerations to explain the factor 2, but there is no analytical proof of this result.

The convergence result in [14] shows two limitations: it does not apply to situations where P_{jk} depends continuously on the distance between the two agents and tends (in particular becomes equal) asymptotically to 0. As a second point, it does not give any idea of how the convergence depends on the total number of agents N; in particular it does not give insight into the double limit behavior $\lim_{t\to+\infty} \lim_{N\to+\infty} x_j(t)$. Since these models are particularly interesting for large values of N, we believe this issue is a crucial one to understand.

The main goal of the present paper is to study the behavior of these models for a large number of agents in any dimension. In order to achieve this, we believe that a fundamental step is to study these dynamical models for continuous distributions of agents. While some considerations in this sense are already given in [3], our point of view is, however, different: we undertake in fact an "Eulerian" point of view, substituting labeled agents with probability measures of agents. Our results (Theorem 1, Proposition 3, and Corollary 4) show that, for a special important case of models preserving global average, the algorithms, in any dimension q and for any finite second moment initial agent distribution, converge to a limit configuration which is always a convex combinations of deltas with reciprocal distance at least R. The core of our convergence results is a Lyapunov stability method: we prove that the second moment of the distribution of agents is a decreasing function of time. At the moment we do

not have (except in the very special symmetric case, Corollary 6) any theoretical tool for predicting the final number of deltas. In the final part of the paper, we present a variety of numerical simulations in 1 and 2 dimensions, obtained by an algorithm stemming from a natural approximation of the Eulerian dynamics. The algorithm is a quantized version of the push-forward mapping (see also [20]); in this respect, it shows analogies with certain classical finite-difference or finite-volume schemes for conservation laws, such as characteristics schemes or upwind schemes. It is quite simple to implement and shows amazing stability properties. As in the cited literature, numerical simulations indicate that only local aggregation takes place and that the limit configuration exhibits more than one delta even if we start from initial distributions with connected support. The actual number of these deltas seems to depend not only on R and on the initial distribution, but also on the specific averaging scheme used.

Our results do not encompass convergence results in [14] but rather complement them, extending convergence to other important models not covered in [14], and above all, they push analysis towards the key direction of distributions of positions (opinions). Our results bring in genuinely new ideas from measure transportation theory and merge them with a Lyapunov stability argument. We believe this type of technique can be applied also to different consensus models (heterogeneous models, gossip models) and will be useful for further progress in this area.

We conclude this section with some further bibliographical notes. Eulerian multiagent systems have also been considered in pedestrian flow models in [19, 20] based on the new modeling perspective proposed in [5].

In the context of multiagent robots, the authors of [7] study modifications of Krause's model, leading to algorithms which have the property of preserving connectivity of the communication graph, and they show that such algorithms converge to consensus. Related papers dealing with coupled second order dynamics have been studied in [8, 9].

1.1. Notation. We report some basic notation used in this paper:

- $|x|$ and $|x|_\infty$ denote, respectively, the Euclidean and the sup norm of $x \in \mathbb{R}^q$;
- $||f||_\infty$ denotes the infinity norm of the $\mathbb{R}^q$-valued function f;
- whenever an integral is on the full domain (typically $\mathbb{R}^q$ or $\mathbb{R}^q \times \mathbb{R}^q$), we will use the simplified symbol $\int$.

2. Assumptions and formulation of the problem. We start by rewriting model (1). We recall that we have a family V of N agents, each of which is the location of an evolution law. We assume that the evolution of all systems takes place over the lattice $0, \tau, 2\tau, \ldots$, where $\tau > 0$ is a fixed time. For the sake of notational simplicity, for every agent $j \in V$, we keep writing $x_j(t)$ for $x_j(\tau t)$ with $t \in \mathbb{N}$. The evolution law of every agent will be written as

$$x_j(t+1) = x_j(t) + \tau u_j(t), \tag{3}$$

where the vector $u_j(t) \in \mathbb{R}^q$ plays the role of a velocity for the evolution of agent j at time t. The velocity law is constructed in the following way. We start from a bounded function $\xi : \mathbb{R}^q \to \mathbb{R}^+$ such that $\xi(x) = \xi(-x)$ for all x, and we put

$$u_j(t) = \frac{1}{N} \sum_{k \in V} \xi(x_k(t) - x_j(t))(x_k(t) - x_j(t)). \tag{4}$$

The coupling of (3) and (4) gives rise to a system as in (1) with

$$P_{jk} = \tau N^{-1} \xi(x_k(t) - x_j(t)).$$

Notice that P is substochastic if $\tau N^{-1} \sum_{k \in V} \xi(x_k(t) - x_j(t)) \leq 1$ for every $j \in V$. An a priori condition which makes this inequality surely hold is $\tau ||\xi||_\infty \leq 1$.

Krause's model (2) does not fit into this framework because of the presence of the normalizing factor, which is not a function of the difference $x_k(t) - x_j(t)$; however, a properly rescaled version of it does fit. It is sufficient to consider

$$\xi(x) = \mathbf{1}_{B(0,R)}(x), \tag{5}$$

where $B(0, R)$ is the closed ball centered in 0 of radius R, and take any $\tau \in]0, 1]$. In other terms, instead of normalizing by $N_j(t)$ (the number of agents with distance R from $x_j(t)$), we normalize by the total number of agents. Numerical simulations with the two models exhibit a very similar structure in their limit configuration; the only difference consists of a minor velocity of the mass transfer observed in our model (5) as opposed to Krause's (2), due to the larger normalization.

An interesting property shared by all models described by (3)–(4) is that the barycenter of the global system is preserved. Indeed, because of the symmetry property $\xi(x) = \xi(-x)$, we immediately see that $\sum_{j \in V} u_j(t) = 0$ for all $t \in \mathbb{N}$. Hence,

$$\frac{1}{N} \sum_{k \in V} x_k(t) = \frac{1}{N} \sum_{k \in V} x_k(0). \tag{6}$$

This property does not hold for (2).

There is a natural continuous-time version of the system we have introduced. It is sufficient to consider $\dot{x}_j(t) = u_j(t)$ where now $t \in \mathbb{R}^+$, with the same choice for the velocities $u_j(t)$ as in (4). In this paper we will not consider the continuous-time model, whose study is deferred to a future paper. Some partial considerations in this direction can be found in [5].

2.1. The Eulerian point of view. When the number of agents N is very large, one can identify the set of agents with a mass distribution μ_t in $\mathbb{R}^q$, which varies in time[1] according to a suitable strategy based on some communication model, as in the previous section. In this identification, borrowing terminology from fluid dynamics, we abandon the "Lagrangian" point of view used above (in which the independent variable j labels individual agents and each of them is observed in its evolution) in favor of an "Eulerian" point of view, in which the independent variable x denotes a point in space occupied at each time by an infinitesimal mass of agents. Since agents are neither created nor destroyed, the total mass of μ_t is preserved, and hence we may assume that μ_t is a probability measure in $\mathbb{R}^q$. As before, the time variable t can be discrete as well as continuous, whereas the model is continuous in space by construction. This means that the mass distribution μ_t can be in principle any Borel probability measure in $\mathbb{R}^q$: for instance, a large number of agents uniformly distributed in an interval $[a, b]$ can be well represented by a normalized Lebesgue measure on $[a, b]$. Another example is the discrete space model of the previous section, which reduces to a particular case of the continuous-space model (see the end of the next section).

[1] Throughout this and subsequent sections, we use the subscript t to denote dependence on time, and not differentiation with respect to t. Similarly, any object $f(t, x)$ depending on both the time variable t and the space variable x will be denoted by $f_t(x)$.

The initial condition is therefore a probability measure μ_0 in $\mathbb{R}^q$ which is assigned and represents the initial spatial configuration of agents.

We start from the model (3)–(4) with $\xi : \mathbb{R}^q \to \mathbb{R}$ assumed to be bounded, measurable, nonnegative, and with the property that $\xi(x) = \xi(-x)$ for all $x \in \mathbb{R}^q$. We now construct the corresponding Eulerian model. To write down the dynamics at the level of probability measures, we suppose that, at time t, we have a mass distribution of agents μ_t. The agents having position (or opinion) $x \in \mathbb{R}^q$ (or, more precisely, the infinitesimal mass of agents $\mu_t(dx)$ at x) move from position x at time t to position $\gamma_t(x)$ at time $t+1$ which, according to the original model (3), we represent as

$$\gamma_t(x) = x + \tau V_t(x). \tag{7}$$

The velocity field $V_t(x)$ has to correspond to the $u_j(t)$'s and we thus choose it as

$$V_t(x) = \int (y - x)\xi(y - x)\, d\mu_t(y) \tag{8}$$

(we recall our standing notational assumption of not indicating the integration domain when it is the full domain).

The mapping $\gamma_t(x)$ which describes how the "mass" is moved by the dynamics allows us, finally, to describe the measure dynamics, by putting

$$\mu_{t+1} = \gamma_t \# \mu_t, \quad t = 0, 1, 2, \ldots, \tag{9}$$

where $\gamma_t\#$ denotes the corresponding action on measures (called the *push-forward* of a measure; see, e.g., [1]). This is formally defined by

$$\gamma_t \# \mu_t(E) = \mu_t(\gamma_t^{-1}(E)) \quad \text{for every Borel set } E; \tag{10}$$

note that the measure μ_{t+1} is completely determined by the identity

$$\int f(x)\, d\mu_{t+1} = \int f(x + \tau V_t(x))\, d\mu_t \tag{11}$$

for every (nonnegative and Borel) function f. Choosing f to be the characteristic function of a set E, for instance, makes this definition consistent with the intuitive idea that a point x in the support of μ_t moves (at time $t+1$) to the point $x + \tau V_t(x)$ in the support of μ_{t+1}.

We now discuss the precise relation of this model with the original model (3)–(4). Straightforward verification shows that if we consider sequences of atomic probability measures

$$\mu_t = \frac{1}{N} \sum_{j \in V} \delta_{x_j(t)}$$

(with $|V| = N$) solving (9), then the trajectories $x_j(t)$ solve (3)–(4).

3. Theoretical results. The main result of this section asserts the convergence of the sequence of measures μ_t.

THEOREM 1. *Let $\xi : \mathbb{R}^q \to \mathbb{R}$ be a nonnegative, bounded, measurable function, satisfying $\xi(x) = \xi(-x)$ for all $x \in \mathbb{R}^q$; assume that $\tau > 0$ is such that $\tau ||\xi||_\infty < 1$.*

Consider the dynamical system (9) *with* γ_t *defined by* (7) *and* (8) *with the initial condition* μ_0 *a probability measure on* $\mathbb{R}^q$ *with finite second moment. Then the sequence of second moments of* μ_t *is nonincreasing, and the sequence of probability measures* μ_t *converges in weak-star sense, as* $t \to \infty$*, to a limit probability measure* μ_∞*, namely,*

$$\lim_{t\to\infty} \int \eta(x)\, d\mu_t(x) = \int \eta(x)\, d\mu_\infty(x)$$

for every continuous test function η *with compact support.*

Remark 2. The weak-star convergence of μ_t to the probability measure μ_∞ can be strengthened a bit if we take into account that second moments are equibounded. In fact, this implies that the family μ_t has moments of any order $p < 2$ which are uniformly integrable, and hence (see, e.g., Proposition 7.1.5 in [1]) it follows that $\mu_t \mapsto \mu_\infty$ with respect to any Wasserstein distance W_p with $p \in [1, 2)$ (the reader is referred to [1] for more details). Further information on the structure of μ_∞ can be obtained, with some extra assumptions on ξ.

PROPOSITION 3. *Suppose that the function* ξ *satisfies the following property: there exist* $R > 0$ *and* $\delta > 0$ *such that* $\xi(x) \geq \delta$ *for every* $x \in \mathbb{R}^q$ *such that* $|x| < R$*. Then,* μ_∞ *is a purely atomic measure, whose atoms are a distance of at least* R *apart from one another.*

Note that, when the assumptions of the above proposition are verified, no matter what the initial measure is, Dirac masses arise in the limit. Hence the weak-star topology is natural in this context and we cannot hope for convergence in total variation.

These results have a straightforward reformulation in terms of the original dynamical system (3)–(4).

COROLLARY 4. *Assume that* ξ *is as above and* $\tau > 0$ *is such that* $\tau||\xi||_\infty < 1$*. Consider the dynamical system* (3)–(4) *with an initial condition* $x_j(0)$*. Then, there exists a subset* Ω *contained in the convex hull of all* $x_j(0)$*'s, such that for every* $j \in V$ *we have that* $x_j(t)$ *converges for* $t \to +\infty$ *to some* $\omega_j \in \Omega$*.*

Moreover, if ξ *satisfies the extra property as in Proposition* 3*, then, if* $\omega_1 \neq \omega_2$ *are both in* Ω*, we have* $|\omega_1 - \omega_2| \geq R$*.*

Proofs of the results above will be obtained in a number of intermediate technical steps.

3.1. The proofs. The following bound, an easy consequence of the Cauchy–Schwarz inequality, will be used later on:

$$\begin{aligned} |V_t(x)|^2 &\leq \int |y-x|^2 \xi(y-x)^2 \, \mathrm{d}\mu_t(y) \\ &\leq \|\xi\|_\infty \int |y-x|^2 \xi(y-x) \, \mathrm{d}\mu_t(y), \quad x \in \mathbb{R}^q. \end{aligned} \tag{12}$$

Note that this bound is useful only if μ_t has finite second order moment.

LEMMA 5. *Suppose that* μ_t *has finite second moment for some* $t \geq 0$*. Then* μ_{t+1} *has finite second moment too, and*

$$\begin{aligned} &\int |x|^2 \, \mathrm{d}\mu_{t+1}(x) - \int |x|^2 \, \mathrm{d}\mu_t(x) \\ &\qquad \leq -\tau(1 - \tau\|\xi\|_\infty) \iint |y-x|^2 \xi(y-x) \, \mathrm{d}\mu_t(y) \, \mathrm{d}\mu_t(x). \end{aligned} \tag{13}$$

Proof. Since μ_t has finite second moment and ξ is bounded, it follows from (12) that $V_t(x) \in L^2(\mathbb{R}^q; \mu_t)$. As a consequence, μ_{t+1} has finite second moment, because

(11) with $f(x) = |x|^2$ yields

$$\begin{aligned}\int |x|^2 \,\mathrm{d}\mu_{t+1}(x) &= \int |x + \tau V_t(x)|^2 \,\mathrm{d}\mu_t(x)\\ &= \int |x|^2 \,\mathrm{d}\mu_t(x) + 2\tau \int x \cdot V_t(x) \,\mathrm{d}\mu_t(x) + \tau^2 \int |V_t(x)|^2 \,\mathrm{d}\mu_t(x),\end{aligned}$$

which can be rewritten as

$$\begin{aligned}&\int |x|^2 \,\mathrm{d}\mu_{t+1}(x) - \int |x|^2 \,\mathrm{d}\mu_t(x)\\ &= 2\tau \int x \cdot V_t(x) \,\mathrm{d}\mu_t(x) + \tau^2 \int |V_t(x)|^2 \,\mathrm{d}\mu_t(x).\end{aligned} \tag{14}$$

Now expanding $V_t(x)$ according to (8) and recalling that $\xi(y - x) = \xi(x - y)$, we obtain

$$\begin{aligned}2\tau \int x \cdot V_t(x) \,\mathrm{d}\mu_t(x) &= 2\tau \iint x \cdot (y - x)\xi(y - x) \,\mathrm{d}\mu_t(y) \,\mathrm{d}\mu_t(x)\\ &= \tau\Bigg(\iint x \cdot (y - x)\xi(y - x) \,\mathrm{d}\mu_t(y) \,\mathrm{d}\mu_t(x)\\ &\qquad + \iint y \cdot (x - y)\xi(x - y) \,\mathrm{d}\mu_t(x) \,\mathrm{d}\mu_t(y)\Bigg)\\ &= -\tau \iint |y - x|^2 \xi(y - x) \,\mathrm{d}\mu_t(y) \,\mathrm{d}\mu_t(x).\end{aligned} \tag{15}$$

On the other hand, using (12) to bound the last integral in (14) we have

$$\tau^2 \int |V_t(x)|^2 \,\mathrm{d}\mu_t(x) \le \tau^2 \|\xi\|_\infty \iint |y - x|^2 \xi(y - x) \,\mathrm{d}\mu_t(y) \,\mathrm{d}\mu_t(x).$$

Finally, plugging the last inequality and (15) into (14), one obtains (13). ∎

COROLLARY 6. *Assume that ξ is as above and $\tau > 0$ is such that $\tau||\xi||_\infty < 1$. If μ_0 has finite second moment, then*

(a) *every μ_t has finite second moment, and the sequence of moments is decreasing;*
(b) *the series of integrals*

$$\sum_{t=0}^{\infty} \iint |x - y|^2 \xi(y - x) \;\mathrm{d}\mu_t(x) \,\mathrm{d}\mu_t(y) \tag{16}$$

is convergent.

Proof. Due to Lemma 5, every μ_t has finite second moment, and the sequence of moments is decreasing due to (13), because by assumption $\tau\|\xi\|_\infty < 1$. Moreover, (13) can be rewritten as

$$\begin{aligned}&\iint |y - x|^2 \xi(y - x) \,\mathrm{d}\mu_t(y) \,\mathrm{d}\mu_t(x)\\ &\le \frac{1}{\tau(1 - \tau\|\xi\|_\infty)} \left(\int |x|^2 \,\mathrm{d}\mu_t(x) - \int |x|^2 \,\mathrm{d}\mu_{t+1}(x)\right).\end{aligned}$$

Summing this inequality over t yields

$$\begin{aligned}&\sum_{t=0}^{T}\iint |y-x|^2\xi(y-x)\,\mathrm{d}\mu_t(y)\,\mathrm{d}\mu_t(x)\\&\le \frac{1}{\tau(1-\tau\|\xi\|_\infty)}\left(\int |x|^2\,d\mu_0(x)-\int |x|^2\,d\mu_T(x)\right)\\&\le \frac{1}{\tau(1-\tau\|\xi\|_\infty)}\int |x|^2\,d\mu_0(x)\end{aligned}$$

and the claim follows since T is arbitrary. ∎

LEMMA 7. *For every test function $\eta\in C^\infty(\mathbb{R}^q)$ having compact support, the limit*

$$\lim_{t\to\infty}\int \eta(x)\,\mathrm{d}\mu_t(x) \tag{17}$$

exists and is finite.

Proof. To prove the result, it suffices to prove that the series

$$\sum_{t=0}^{\infty}\left|\int \eta(x)\,\mathrm{d}\mu_{t+1}(x)-\int \eta(x)\,\mathrm{d}\mu_t(x)\right| \tag{18}$$

is convergent (indeed, in this case the series obtained by removing the absolute values is still convergent, which means that the limit in (17) exists and is finite).

Let

$$H=\|D^2\eta\|_\infty$$

be the sup norm of the Hessian matrix of η. According to (11), we have for every $t\ge 0$

$$\int \eta(x)\,\mathrm{d}\mu_{t+1}(x)-\int \eta(x)\,\mathrm{d}\mu_t(x)=\int\big(\eta(x+\tau V_t(x))-\eta(x)\big)\,\mathrm{d}\mu_t(x). \tag{19}$$

On the other hand, for $x,z\in\mathbb{R}^q$ we have by Taylor's formula

$$\eta(x+z)-\eta(x)=\nabla\eta(x)\cdot z+R(x,z),$$

where the error $R(x,z)$ satisfies the estimate

$$|R(x,z)|\le H\,|z|^2. \tag{20}$$

If we plug this expansion into (19) with the choice $z=\tau V_t(x)$, we obtain

$$\begin{aligned}&\int \eta(x)\,\mathrm{d}\mu_{t+1}(x)-\int \eta(x)\,\mathrm{d}\mu_t(x)\\&\quad=\tau\int \nabla\eta(x)\cdot V_t(x)\,\mathrm{d}\mu_t(x)+\int R(x,\tau V_t(x))\,\mathrm{d}\mu_t(x),\end{aligned}$$

and hence using first (20) and then (12) we obtain

$$\begin{aligned}&\left|\int \eta(x)\,\mathrm{d}\mu_{t+1}(x)-\int \eta(x)\,\mathrm{d}\mu_t(x)\right|\\&\le\tau\left|\int \nabla\eta(x)\cdot V_t(x)\,\mathrm{d}\mu_t(x)\right|\\&\qquad+H\tau^2\|\xi\|_\infty\iint |y-x|^2\xi(y-x)\,\mathrm{d}\mu_t(y)\,\mathrm{d}\mu_t(x).\end{aligned} \tag{21}$$

To estimate the integral involving $\nabla\eta$, we express $V_t(x)$ according to (8) to find

$$\begin{aligned}&\int \nabla\eta(x)\cdot V_t(x)\,\mathrm{d}\mu_t(x)\\&= \iint \nabla\eta(x)\cdot(y-x)\xi(y-x)\,\mathrm{d}\mu_t(y)\,\mathrm{d}\mu_t(x)\\&= \frac{1}{2}\iint \big(\nabla\eta(x)-\nabla\eta(y)\big)\cdot(y-x)\xi(y-x)\,\mathrm{d}\mu_t(y)\,\mathrm{d}\mu_t(x)\end{aligned}$$

(the last inequality follows from the general fact that $\iint F(x,y)\,\mathrm{d}\mu_t(y)\,\mathrm{d}\mu_t(x) = \iint F(y,x)\,\mathrm{d}\mu_t(y)\,\mathrm{d}\mu_t(x)$, because the measure $\mu_t\otimes\mu_t$ is symmetric about the diagonal, combined with the property $\xi(x-y)=\xi(y-x)$). But the function $\nabla\eta$ is Lipschitz continuous with constant H, and hence we have the estimate

$$\left|\int \nabla\eta(x)\cdot V_t(x)\,\mathrm{d}\mu_t(x)\right| \le H\iint |x-y|^2\xi(y-x)\,\mathrm{d}\mu_t(x)\,\mathrm{d}\mu_t(y)$$

which, plugged into (21), yields

$$\begin{aligned}&\left|\int \eta(x)\,\mathrm{d}\mu_{t+1}(x) - \int \eta(x)\,\mathrm{d}\mu_t(x)\right|\\&\le H(\tau+\tau^2\|\xi\|_\infty)\iint |y-x|^2\xi(y-x)\,\mathrm{d}\mu_t(y)\,\mathrm{d}\mu_t(x).\end{aligned}\tag{22}$$

Summing over t and using Corollary 6, we finally obtain that the series in (18) is convergent. ∎

We are now ready to prove the convergence result.

Proof of Theorem 1. From Lemma 7, we know that the probability measures μ_t converge, in the sense of distributions, to some distribution μ_∞. But since μ_∞ is nonnegative, it is necessarily a Radon measure in $\mathbb{R}^q$ by the Riesz representation theorem. Moreover, by semicontinuity of the total variation, we have $\mu_\infty(\mathbb{R}^q)\le 1$. To prove that equality occurs, it suffices to show that the family of probability measures μ_t is precompact. By well-known results (see, e.g., [1, pp. 108–109]), this follows immediately from (13), which shows that the second moment of μ_t is nonincreasing with respect to t (and hence moments are equibounded). ∎

Proof of Proposition 3. We start by observing that, if μ_t converges (in the weak-star topology of measures) to μ_∞, then the product measures $\mu_t\otimes\mu_t$ (thought of as measures on $\mathbb{R}^{2q}=\mathbb{R}^q\times\mathbb{R}^q$) converge to $\mu_\infty\otimes\mu_\infty$. Then, since moments of the second order are equibounded, μ_∞ has finite second order moment, and we can pass to the limit in the following integral:

$$\iint |x-y|^2\xi(y-x)\,d\mu_\infty(x)d\mu_\infty(y) = \lim_{t\to\infty}\iint |x-y|^2\xi(y-x)\,d\mu_t(x)d\mu_t(y).$$

But, since the series in (16) is convergent, this limit is zero, i.e.,

$$\iint |x-y|^2\xi(y-x)\,\mathrm{d}\mu_\infty(x)\mathrm{d}\mu_\infty(y) = 0.$$

Now take any two distinct points $x,y\in\mathbb{R}^q$, both in the support of μ_∞ (if no such pair of points exists, then the support of μ_∞ reduces to a single point; i.e., μ_∞ is a single Dirac mass). It is a general fact that $(x,y)\in\mathbb{R}^q\times\mathbb{R}^q$ belongs to the support of the

product measure $\mu_\infty \otimes \mu_\infty$. If $|x-y| < R$, then since $x \neq y$ and by the assumption made on ξ, we have that

$$|y-x|^2 \xi(y-x) > 0,$$

and the same inequality holds in some neighborhood A of (x,y). But since (x,y) belongs to the support of $\mu_\infty \otimes \mu_\infty$, we obtain

$$\begin{aligned} &\iint |x-y|^2 \xi(y-x)\, d\mu_\infty(x) \mathrm{d}\mu_\infty(y) \\ &\geq \iint_A |x-y|^2 \xi(y-x)\, d\mu_\infty(x) \mathrm{d}\mu_\infty(y) > 0, \end{aligned}$$

a contradiction. Then, necessarily, $|x-y| \geq R$ whenever x, y are two distinct points in the support of μ_∞. It follows that the support of μ_∞ is a discrete set of points with mutual distances at least R. ∎

4. Symmetries. We are not able, in general, to predict the number of deltas which will appear in the limit configuration starting from a given initial measure μ_0 (even when μ_0 is the uniform distribution). However, some further information on μ_∞ can be obtained in the presence of symmetries.

We have the following result.

PROPOSITION 8. *Consider an isometry $T : \mathbb{R}^q \to \mathbb{R}^q$ with $T(x) = Ux + b$ for some orthogonal matrix U and vector $b \in \mathbb{R}^q$. Assume that ξ is U-invariant ($\xi \circ U = \xi$). If μ_t is the solution of* (9) *with respect to the initial condition μ_0, then $T\#\mu_t$ is the solution of* (9) *with respect to the initial condition $T\#\mu_0$.*

Proof. Define

$$W_t(x) = \int (y-x)\xi(y-x)\, \mathrm{d}(T\#\mu_t)(y).$$

It follows from the U-invariance of ξ and the definition of push-forward measure that, for all $x \in \mathbb{R}^q$,

$$\begin{aligned} W_t(T(x)) &= \int (y - T(x))\xi(y - T(x))\, \mathrm{d}(T\#\mu_t)(y) \\ &= \int (T(y) - T(x))\xi(T(y) - T(x))\, \mathrm{d}\mu_t(y) \\ &= U \int (y-x)\xi(y-x)\, \mathrm{d}\mu_t(y) = UV_t(x). \end{aligned}$$

Notice now that

$$\begin{aligned} &\int f(x)\, \mathrm{d}(T\#\mu_{t+1})(x) = \int f(T(x))\, \mathrm{d}\mu_{t+1}(x) \\ &= \int f(T(x + V_t(x)))\, \mathrm{d}\mu_t(x) = \int f(T(x) + UV_t(x))\, \mathrm{d}\mu_t(x) \\ &= \int f(T(x) + W_t(T(x)))\, \mathrm{d}\mu_t(x) \\ &= \int f(x + W_t(x))\, \mathrm{d}(T\#\mu_t)(x), \end{aligned}$$

which proves the claim. ∎

This has some interesting consequences.

COROLLARY 9. *Consider an isometry $T : \mathbb{R}^q \to \mathbb{R}^q$ with $T(x) = Ux + b$, and assume that ξ is U-invariant ($\xi \circ U = \xi$). Then,*

$$T\#\mu_0 = \mu_0 \Rightarrow T\#\mu_\infty = \mu_\infty.$$

A probability measure μ is said to have a radial symmetry with respect to $x_0 \in \mathbb{R}^q$ if for any rotation T centered in x_0 we have that $T\#\mu = \mu$. We can now present our last result.

COROLLARY 10. *Let ξ be a radial function and let $V_t(x)$ be given by* (8). *If μ_0 has radial symmetry with respect to x_0, then $\mu_\infty = \delta_{x_0}$.*

Proof. By Corollary 9, we have that μ_∞ also has radial symmetry with respect to x_0, and since it must be a finite combination of deltas, it has to coincide with δ_{x_0}. ∎

5. A numerical algorithm. In this section, we introduce a spatially discrete Eulerian measure dynamics, which approximates the dynamics described by (9). A numerical algorithm is then naturally associated with it and will be detailed hereafter. In the next section, through numerical simulations in 1 and 2 dimensions we will apply the algorithm to provide some insight into the actual asymptotic behavior of the solutions of our model.

The algorithm we are going to describe can be interpreted as a simple characteristics scheme in the language of finite-difference methods for classical conservation laws, or as a particular upwind scheme in the language of finite-volume methods. In our opinion, what is perhaps remarkable and of some interest is its direct connection with the push-forward of measures, a powerful tool which allows one to extend the concept of conservation law beyond the classical framework. Indeed, on the basis of the new theoretical perspective introduced in our previous paper [5], other authors [20] have developed an analogous algorithm and applied it to the modeling of pedestrian flows. Some of the properties of the algorithm that we just mention below have been thoroughly investigated in [20], to which we refer the reader for further details.

We denote by $m(A)$ the Lebesgue measure of a measurable set A. Let us introduce a partition $\mathcal{D}$ of $\mathbb{R}^q$ made of mutually disjoint, bounded Borel sets D. Given any $E \in \mathcal{D}$, we have by (10)

$$\mu_{t+1}(E) = \mu_t\left(\gamma_t^{-1}(E)\right) = \sum_{D\in\mathcal{D}} \mu_t\left(D \cap \gamma_t^{-1}(E)\right). \tag{23}$$

Now, we make the following assumptions:

(i) In each $D \in \mathcal{D}$, μ_t is approximated by a multiple of the Lebesgue measure therein; i.e., there exists a nonnegative constant ρ_t^D such that

$$\mu_{t|D} \sim \rho_t^D dx_{|D}; \tag{24}$$

the mass density ρ_t^D is uniquely determined by the condition $\mu_t(D) = \rho_t^D \int_D dx$, whence $\rho_t^D = \mu_t(D)/m(D)$.

(ii) In each $D \in \mathcal{D}$, γ_t is approximated by an affine invertible mapping γ_t^D; more precisely, we assume that in D the velocity V_t is approximated by a constant velocity V_t^D, so that γ_t^D is defined by

$$\gamma_t^D(x) = x + \tau V_t^D. \tag{25}$$

Note that such a γ_t^D is but a translation parallel to the axes, so that $m(X) = m(\gamma_t^D(X))$ for any measurable $X \subseteq D$ (see Figure 1).

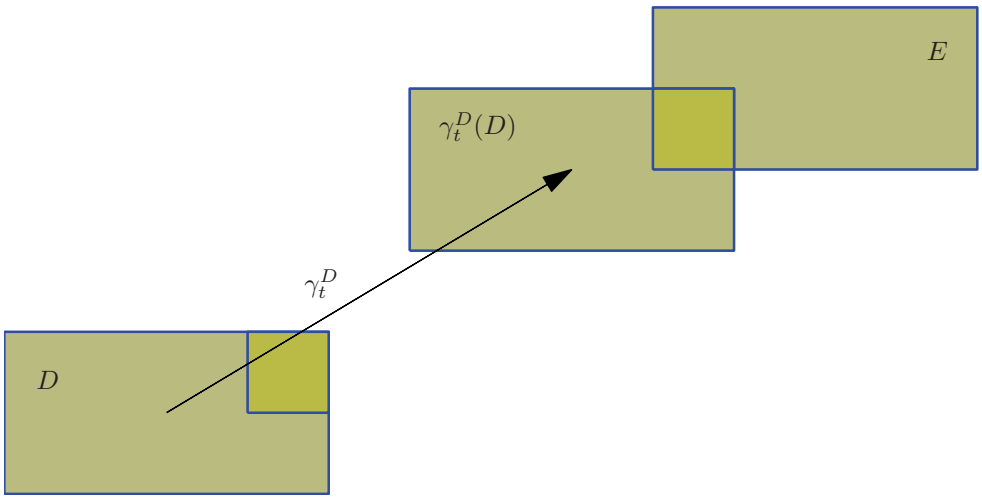

FIG. 1. *Pictorial representation of the "push-forward" algorithm.*

Using these approximations in (23), we obtain

$$\mu_{t+1}(E) = \rho_{t+1}^E m(E) \sim \sum_{D\in\mathcal{D}} \rho_t^D m(D \cap \left(\gamma_t^D\right)^{-1}(E)) = \sum_{D\in\mathcal{D}} \rho_t^D m(\gamma_t^D(D) \cap E),$$

which provides the following discrete counterpart of (9), i.e., the approximate dynamics for the local mass densities:

$$\rho_{t+1}^E \sim \sum_{D\in\mathcal{D}} \frac{m(\gamma_t^D(D)\cap E)}{m(E)}\,\rho_t^D \qquad \forall E \in \mathcal{D}. \tag{26}$$

Note that this expression and Figure 1 suggest an analogy between the numerical algorithm we are going to introduce and a (forward) characteristic scheme for the finite-difference discretization of the scalar conservation law

$$\frac{\partial}{\partial t}\rho_t + \operatorname{div}(V_t\rho_t) = 0. \tag{27}$$

The algorithm is obtained by specifying the partition $\mathcal{D}$ and the choice of the velocities V_t^D, and by equating the left-hand side to the right-hand side in the previous approximate relation.

Given any step-size $h > 0$, consider the lattice $x_j = jh$, with $j = (j_1, \dots, j_q) \in \mathbb{Z}^q$, and define the cells

$$\bar{D}_j = x_j + h[-1/2, 1/2]^q$$

centered at x_j; for the sake of simplicity, from now on let us write ρ_t^j for $\rho_t^{D_j}$ and similarly for all other variables. The approximate velocity in the cell D_j is defined as $V_t^j = V_t(x_j)$, where, according to (8), we set

$$V_t(x_j) = \sum_{k\in\mathbb{Z}^q} \int_{D_k} (y - x_j)\xi(y - x_j)\rho_t^k dy.$$

With these definitions, we consider the following algorithm:

$$\rho_{t+1}^j = \sum_{k\in\mathbb{Z}^q} \frac{m(\gamma_t^k(D_k)\cap D_j)}{m(D_j)}\,\rho_t^k \qquad \forall j\in\mathbb{Z}^q. \tag{28}$$

Remark 11. This algorithm guarantees local (hence, global) conservation of mass. Indeed, the local mass $\rho_t^k m(D_k)$ contained at time t in the cell D_k contributes to the local mass in the cell D_j at time $t+1$ by the quantity

$$\frac{m(\gamma_t^k(D_k)\cap D_j)}{m(D_j)}\,\rho_t^k m(D_j) = m(\gamma_t^k(D_k)\cap D_j)\rho_t^k;$$

summing up over j, one has

$$\sum_{j\in\mathbb{Z}^q} m(\gamma_t^k(D_k)\cap D_j)\rho_t^k = m(\gamma_t^k(D_k))\rho_t^k = m(D_k)\rho_t^k,$$

which expresses the desired conservation property.

Remark 12. The piecewise constant approximations introduced above in (i) and (ii) lead to a first order consistency error in h and τ. Obviously, higher order approximations are possible. In particular, as far as (24) is concerned, one could look for a polynomial density function ρ_t^D, say $\rho_t^D\in\mathbb{Q}_r(D)$ (the space of polynomials over D of degree $\le r$ in each spatial variable); in this case, we require exactness of the moments of μ_t up to the order r, i.e.,

$$\int_D x^m d\mu_t = \int_D x^m \rho_t^D dx \qquad \forall x^m\in\mathbb{Q}_r(D).$$

Similarly, in (25) the constant V_t^D could be replaced by a higher order polynomial function, provided the resulting map γ_t^D remains invertible.

Finally, from now on we assume that the time step τ is chosen in such a way that the following Courant–Friedrichs–Lewy (CFL) condition is fulfilled for each t:

$$\frac{\tau}{h}\max_{k\in\mathbb{Z}^q}|V_t^k|_\infty \le 1, \tag{29}$$

where $|\cdot|_\infty$ denotes the maximum norm in $\mathbb{R}^q$. This choice simplifies our scheme, in that the image $\gamma_t^k(D_k)$ of the cell D_k is just contained in the union of the 3^q cells D_j having $|j-k|_\infty\le 1$. Thus, the algorithm described in (28) can be made more precise as follows:

$$\rho_{t+1}^j = \sum_{k\,:\,\|j-k\|_\infty\le 1} \frac{m(\gamma_t^k(D_k)\cap D_j)}{m(D_j)}\,\rho_t^k \qquad \forall j\in\mathbb{Z}^q. \tag{30}$$

Obviously, condition (29) is not mandatory for the stability of our scheme: a less stringent choice of τ is indeed admissible, provided the numerical domain of dependence of each cell at time $t+1$ is allowed to be as large as needed. However, one has to remember that assumption (ii) above yields sufficiently accurate results only if τ is small enough.

Example 1. Let us detail the 1D version of the above algorithm. To this end, let us set $\lambda=\frac{\tau}{h}$, and let us observe that for any $k\in\mathbb{Z}$,

$$\gamma_t^k(D_k)\cap D_{k-1} = \begin{cases} (x_{k-1/2}+\tau V_t^k, x_{k-1/2}) & \text{if } V_t^k<0,\\ \emptyset & \text{if } V_t^k\ge 0,\end{cases}$$

whence

$$\frac{m(\gamma_t^k(D_k)\cap D_{k-1})}{m(D_{k-1})} \;=\; \begin{cases} -\lambda V_t^k & \text{if } V_t^k<0,\\ 0 & \text{if } V_t^k\geq 0,\end{cases} \;=\; \lambda(V_t^k)_-, \tag{31}$$

where $x_+=\max(x,0)$ and $x_-=\max(0,-x)$ denote as usual the positive and negative parts of the number x. Similarly,

$$\gamma_t^k(D_k)\cap D_{k+1}=\begin{cases}\emptyset & \text{if } V_t^k\leq 0,\\ (x_{k+1/2},x_{k+1/2}+\tau V_t^k) & \text{if } V_t^k>0,\end{cases}$$

whence

$$\frac{m(\gamma_t^k(D_k)\cap D_{k+1})}{m(D_{k+1})} \;=\; \begin{cases} 0 & \text{if } V_t^k\leq 0,\\ \lambda V_t^k & \text{if } V_t^k>0,\end{cases} \;=\; \lambda(V_t^k)_+. \tag{32}$$

Finally,

$$\gamma_t^k(D_k)\cap D_k=\begin{cases}(x_{k-1/2},x_{k+1/2}+\tau V_t^k) & \text{if } V_t^k\leq 0,\\ (x_{k-1/2}+\tau V_t^k,x_{k+1/2}) & \text{if } V_t^k\geq 0,\end{cases}$$

whence

$$\frac{m(\gamma_t^k(D_k)\cap D_k)}{m(D_k)} \;=\; \begin{cases} 1+\lambda V_t^k & \text{if } V_t^k\leq 0,\\ 1-\lambda V_t^k & \text{if } V_t^k\geq 0,\end{cases} \;=\; 1-\lambda(V_t^k)_- -\lambda(V_t^k)_+. \tag{33}$$

We now use (31) with $k=j+1$, (32) with $k=j-1$, and (33) with $k=j$. Substituting into (30) and setting, for the sake of simplicity,

$$\begin{aligned} c_m &= \lambda(V_t^{j-1})_+,\\ c_0 &= 1-\lambda(V_t^j)_- -\lambda(V_t^j)_+,\\ c_p &= \lambda(V_t^{j+1})_-, \end{aligned} \tag{34}$$

we immediately obtain the scheme

$$\rho_{t+1}^j = c_m\,\rho_t^{j-1}+c_0\,\rho_t^j+c_p\,\rho_t^{j+1} \qquad \forall j\in\mathbb{Z}. \tag{35}$$

Note that if the velocities are of constant sign, then the scheme reduces to

$$\rho_{t+1}^j=\rho_t^j-\begin{cases}\lambda(V_t^j\rho_t^j-V_t^{j-1}\rho_t^{j-1}) & \text{(positive velocities)},\\ \lambda(V_t^{j+1}\rho_t^{j+1}-V_t^j\rho_t^j) & \text{(negative velocities)};\end{cases} \tag{36}$$

i.e., the scheme can be regarded as a finite-volume upwind scheme [13] applied to the conservation law

$$\frac{\partial}{\partial t}\rho_t+\frac{\partial}{\partial x}(V_t\rho_t)=0.$$

Example 2. By exploiting the tensor-product structure of the grid, the 2D version of our algorithm is easily obtained from the 1D version. Indeed, for any $j=(j_1,j_2)\in\mathbb{Z}^2$, one has

$$\begin{aligned} \rho_{t+1}^{(j_1,j_2)} &= c_{mm}\,\rho_t^{(j_1-1,j_2-1)} + c_{0m}\,\rho_t^{(j_1,j_2-1)} + c_{pm}\,\rho_t^{(j_1+1,j_2-1)}\\ &+ c_{m0}\,\rho_t^{(j_1-1,j_2)} + c_{00}\,\rho_t^{(j_1,j_2)} + c_{p0}\,\rho_t^{(j_1+1,j_2)}\\ &+ c_{mp}\,\rho_t^{(j_1-1,j_2+1)} + c_{0p}\,\rho_t^{(j_1,j_2+1)} + c_{pp}\,\rho_t^{(j_1+1,j_2+1)}, \end{aligned} \tag{37}$$

where each coefficient $c_{\alpha\beta} = c_\alpha c_\beta$, with $\alpha, \beta \in \{m, 0, p\}$, is the product of two 1D coefficients defined as in (34) through the values of the x- and y-components of the velocity, respectively; each coefficient is computed in the cell indicated by the associated mass density. Thus, the scheme is equivalent to a genuinely multidimensional version of the upwind scheme for the conservation law (27); here, the expression "genuinely multidimensional" refers to the fact that the numerical fluxes of a given cell (whose sides are always aligned with the coordinate axes) are updated by considering neighboring cells not only in the horizontal and vertical directions, but also in the oblique directions. Our experience indicates that this feature is essential for approximating the formation of an atomic measure, for otherwise the resulting algorithm turns out to be both inaccurate and nonrobust.

The extension to 3 or more dimensions is straightforward. More generally, replacing densities by measures, our scheme can be viewed as a space-time discretization of the continuous-time, continuous-space model

$$\frac{\partial}{\partial t}\mu_t + \operatorname{div}(V_t \mu_t) = 0, \tag{38}$$

which governs the evolution of the mass distributions μ_t when the time variable t varies continuously rather than discretely. This equation must be thought of in the sense of measures. Formally, if we multiply (38) by a smooth test function $\eta(x)$ with compact support, and we integrate in space (by part in the last term), we obtain

$$\frac{d}{dt}\int \eta(x)\, d\mu_t(x) = \int \nabla\eta(x) \cdot V_t(x)\, d\mu_t(x). \tag{39}$$

This suggests the following notion of solution. We say that a family of probability measures μ_t, $t \geq 0$, is a solution of (38) if for every test function $\eta(x)$, continuous with compact support in $\mathbb{R}^q$, the function

$$t \mapsto \int \eta(x)\, d\mu_t(x), \quad t \geq 0,$$

is absolutely continuous in $[0, \infty)$ and satisfies (39) for almost every $t > 0$. Note that this definition makes sense for every initial probability measure μ_0.

The study of continuous-time models will be detailed elsewhere.

6. Simulations. In this section, we illustrate the behavior of our model through a variety of numerical simulations obtained by the algorithm described above. We consider the 1D and 2D cases separately.

With any choice of initial measure μ_0, cut-off function ξ, and mesh spacing h, the algorithm generates a sequence of measures whose densities are piecewise constant on the chosen mesh. As $t \to \infty$, the subsequent experiments clearly indicate that they converge to a steady state, represented by a finite distribution of "discrete deltas" which agree with the statement of Proposition 3; i.e., they are a distance of at least R apart from each other. We conjecture that perhaps a nontrivial adaptation of the arguments given in section 3.1 could lead to a rigorous proof of this fact.

We refer to [2, 3] for related simulations based on the 1D model; 2D simulations, although in a different context than ours, can be found in [15].

6.1. 1D simulations. The first set of simulations is relative to the initial measure μ_0 whose density is the characteristic function of the interval $[0.5, 1.5]$. We report the results for two choices of the weight function ξ: (i) the characteristic function $\xi_{1,R}$

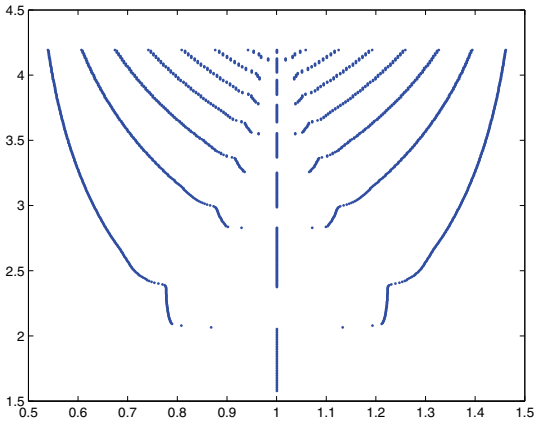

FIG. 2. *Position of discrete deltas versus* $\log(1/R)$ *(with* $h = 1/1600$*) for the piecewise constant initial density.*

of the interval $[-R, R]$; (ii) the piecewise linear hat function $\xi_{2,R}(z) = 1 - |z|/R$. In both cases, the observed asymptotic dynamics is consistent with the theoretical prediction of Proposition 3; i.e., a finite number of deltas is created whose minimal distance is invariably larger than R. Figure 2, obtained with $\xi = \xi_{1,R}$ and $h = 1/1600$, provides a sort of "bifurcation diagram" in which the position of the discrete deltas in the interval $[0.5, 1.5]$ (represented on the horizontal axis) is plotted against $\log(1/R)$ (represented on the vertical axis). This scenario appears to be quite robust with respect to numerical discretization errors. Similar diagrams have been reported in the recent literature (see [2] and the references therein), stemming from related but different models.

Next, we investigate the influence of the weight ξ on the asymptotic patterns. For both choices $\xi = \xi_{1,R}$ and $\xi = \xi_{2,R}$ and several values of R, we have monitored the number $\#\delta$ of deltas, as well as the interdelta distance, expressed by the ratios $\sigma_{\min} = d_{\min}/R$ and $\sigma_{\max} = d_{\max}/R$, where $d_{\min}$ and $d_{\max}$ are the minimal and maximal distance between two consecutive deltas. Indeed, it is conjectured in the literature mentioned above that this ratio should be around 2. Our results, given in Table 1, suggest the existence of a limit intradelta distance significantly larger than R, yet they also indicate a clear dependence on the particular weight assigned to the neighboring agents in the communication graph.

TABLE 1
Number of deltas and intradelta distance as a function of R.

	$\xi = \xi_{1,R}$			$\xi = \xi_{2,R}$		
R	$\#\delta$	$\sigma_{\min}$	$\sigma_{\max}$	$\#\delta$	$\sigma_{\min}$	$\sigma_{\max}$
0.10	4	2.367	2.450	5	1.800	2.175
0.08	5	2.250	2.635	7	1.646	1.802
0.06	7	2.250	2.472	9	1.792	1.930
0.04	11	2.167	2.250	14	1.583	1.812
0.02	22	2.208	2.333	28	1.583	1.792

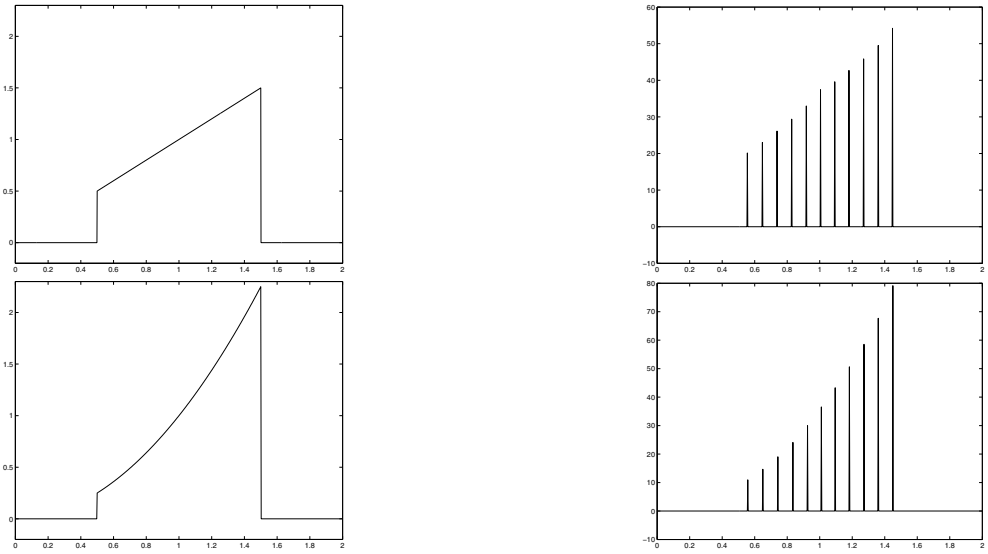

FIG. 3. *Initial piecewise linear density (top left); discrete deltas at convergence (top right); initial piecewise parabolic density (bottom left); discrete deltas at convergence (bottom right).*

Finally, we consider two nonconstant initial distributions, a linear and a parabolic one given by the left-hand plots of Figure 3. The resulting patterns of discrete deltas, obtained at convergence for $R = 0.04$ with $\xi = \xi_{1,R}$ and $h = 1/800$, are shown in the corresponding right-hand plots. The figures show a characteristic feature of the communication model under investigation; namely, the mass transportation occurs only locally (on a scale proportional to R) but not globally (on the scale of the support of the initial density). Indeed, the strengths of the limit deltas retain the linear or parabolic behavior of the initial data. The "bifurcation" diagram for such cases (see Figure 4) indicates that the loss of symmetry does not destroy the mechanism of one-by-one increment of the number of deltas as R decreases, observed above. The ratios $\sigma_{\min}$ and $\sigma_{\max}$ are 2.125 and 2.292 (linear case) and 2.066 and 2.312 (parabolic case).

6.2. 2D simulations. As in the 1D situations, we start from an initial measure μ_0 whose density is the characteristic function of a bounded connected subset of the plane: a square (Figure 5), a "horseshoe" or "Π-like" domain (Figure 6), and a disk (Figure 7). Such initial supports are represented by the dashed lines in these figures. We apply the algorithm described in section 5, using as cut-off function ξ the characteristic function of the closed ball $B(0, R) \subseteq \mathbb{R}^q$; the definition actually depends upon the choice of the norm used to define the ball: let $\xi_{2,R}$ be the cut-off function defined via the Euclidean norm $|z|$, and let $\xi_{\infty,R}$ denote the function associated with the maximum norm $|z|_\infty$.

The typical pattern of the limit densities is illustrated in Figure 8: in the most generic situation, we find a cluster of four contiguous cells carrying nonzero densities, surrounded by cells with vanishing density. It is easily seen that any combination of values of the four nonzero densities is compatible with the time invariance of the pattern, so the actual values depend on the initial mass and the evolution of the discrete dynamical system. We are indeed able to prove that no limit pattern with more than four contiguous cells is allowed, since such a configuration would induce

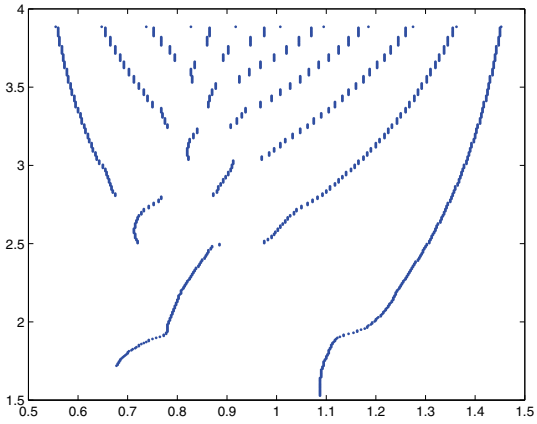

FIG. 4. *Position of discrete deltas versus* $\log(1/R)$ *(with* $h = 1/1600$*) for the piecewise linear initial density.*

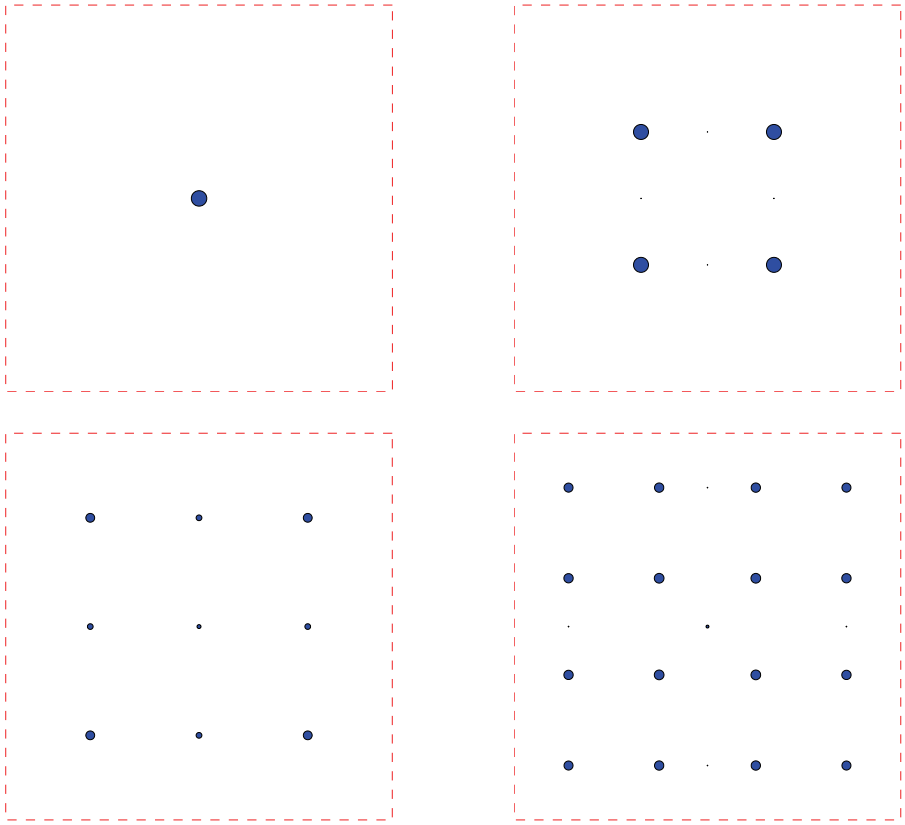

FIG. 5. *The square case for* $h = 1/64$*. Top left:* $R = 0.30$*; top right:* $R = 0.23$*; bottom left:* $R = 0.15$*; bottom right:* $R = 0.10$*.*

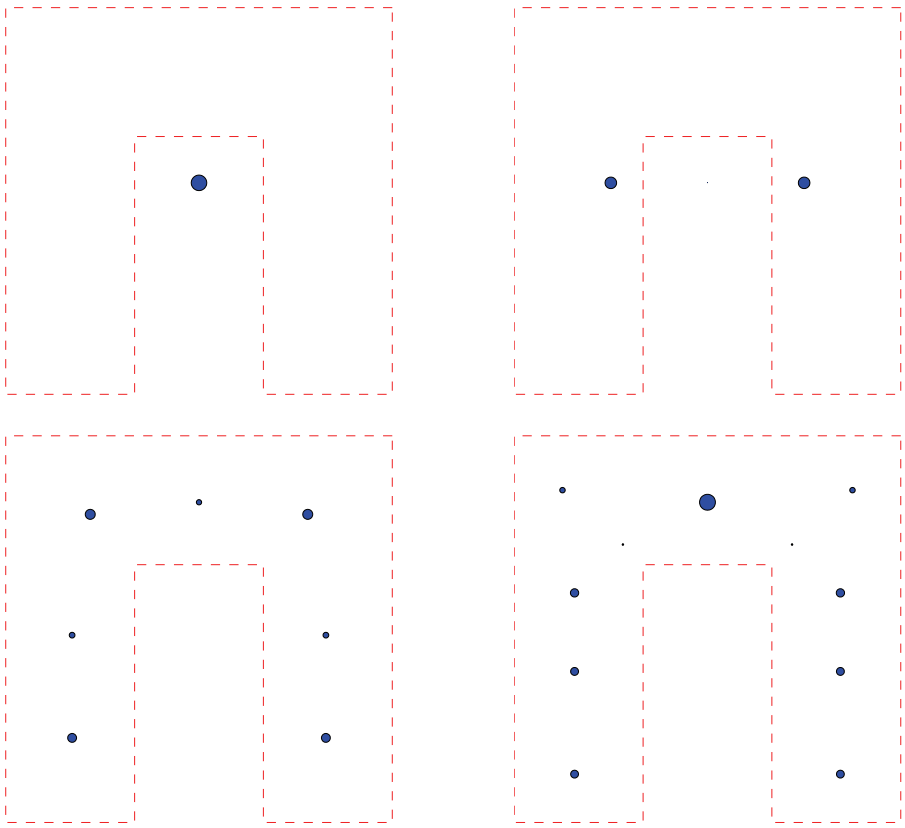

FIG. 6. *The horseshoe case for* $h = 1/64$. *Top left:* $R = 0.40$*; top right:* $R = 0.30$*; bottom left:* $R = 0.15$*; bottom right:* $R = 0.08$.

an unsteady mass transportation from the outer cells towards the center; the proof will appear elsewhere, together with other theoretical properties of the algorithm. On the other hand, symmetries may lead to a simplification of the limit pattern. Indeed, for a mesh-size $h = 1/N$, we use $2N + 1$ cells in each space direction; hence, the $(N + 1)$th cell is symmetrically placed, and an initial symmetric distribution of mass with respect to this cell is preserved. Thus, symmetry in the vertical (resp., horizontal) direction leads to a limit pattern made of only two contiguous cells, placed along the horizontal (resp., vertical) direction. Symmetry in both directions leads to a unique limit cell. This is clearly documented in Figure 8.

Once a limit pattern has been detected, we associate to it a "discrete delta" of the form $a\delta_{x_0}$; the point x_0 is computed as the center of mass of the pattern, whereas the coefficient a is the sum of the mass carried by the pattern, multiplied by h^2. Graphically, any such delta is represented, in all of the plots which form Figures 5–7, by a dark circle, centered at x_0 and having a radius proportional to a. Note that the proportionality factor is the same for all deltas of the same plot, but it varies (for aesthetic reasons only) from one plot to another; in other words, it is meaningful to compare the "strength" of different deltas only within the same plot.

While Figures 5–7 show the limit distributions of deltas on a fixed mesh ($h = 1/64$) as R varies, it is also interesting to investigate mesh convergence for a fixed value of

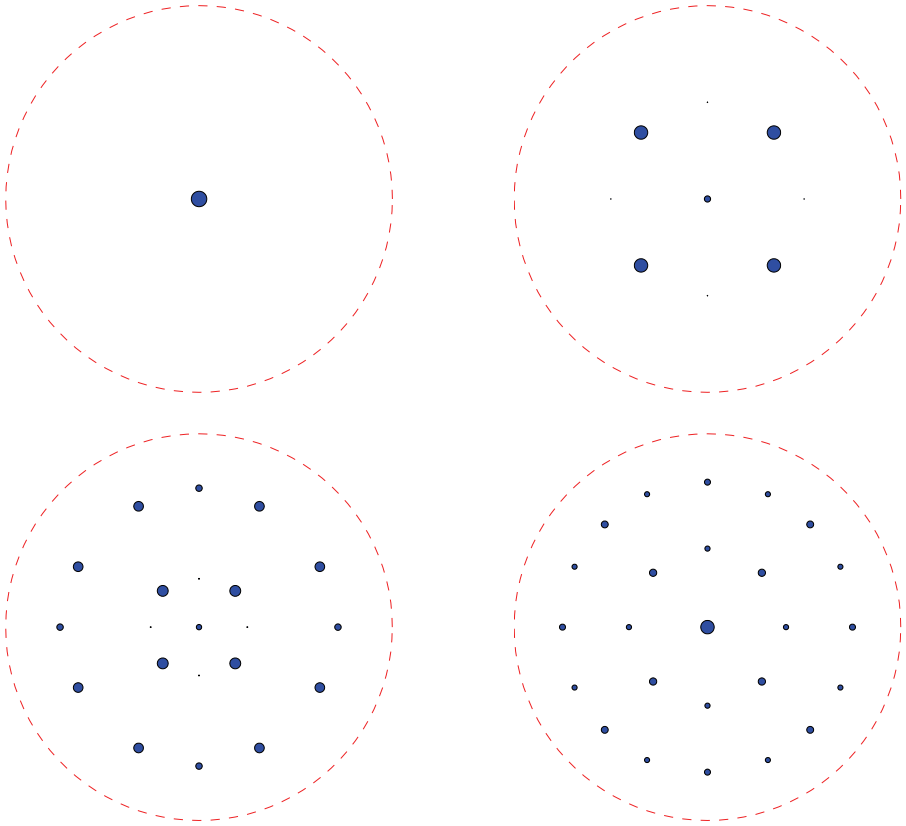

FIG. 7. *The disk case for* $h = 1/64$. *Top left:* $R = 0.30$*; top right:* $R = 0.15$*; bottom left:* $R = 0.10$*; bottom right:* $R = 0.08$.

TABLE 2

The square case for $R = 0.15$*: concentrated measures* $a\delta$ *at shown locations. Approximate values of the constants* a *versus* h.

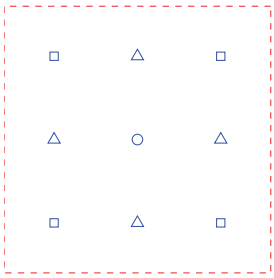

$1/h$	◯	△	□
16	0.087	0.107	0.124
32	0.040	0.079	0.162
64	0.064	0.092	0.142
128	0.093	0.103	0.122
256	0.095	0.106	0.120

R. This is presented in Table 2, where the dependence of a upon h is reported for the distribution of deltas shown in the figure on the left-hand side. Apart from the initial case $h = 1/16$, which probably corresponds to a mesh too coarse to capture the asymptotic features of the exact dynamical system, for the other values of h, mesh convergence is clearly documented.

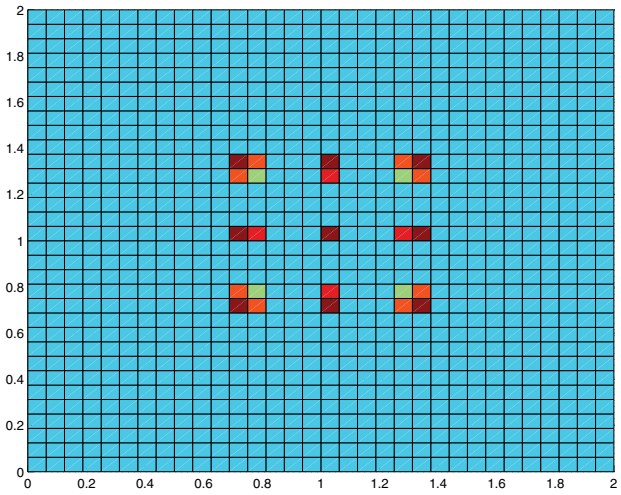

FIG. 8. *The square case for* $R = 0.15$ *and* $h = 1/16$*: structure of the limit densities.*

Finally, we comment on Figures 5–7: globally speaking, they indicate the occurrence of a "bifurcation diagram" of concentrated measures, similar to those given in one dimension; obviously, in two dimensions symmetries force more than one delta to be simultaneously created as R exceeds a certain critical value. The square case (Figure 5) is the most evident from this point of view, with the transition from 1 to 4 deltas, followed by 9–16 deltas, as R decreases. Note that the small deltas which appear along the median axes in the plots on the right-hand side are numerically spurious (i.e., their strength a tends to zero as $h \to 0$): they collect all of the mass initially contained in the cells placed along the median axes, a mass that by symmetry cannot be attracted by any of the other deltas. We also note that the distance between contiguous deltas is by far larger than R, ranging around $2R$ or more, as in the 1D case.

Figure 6 provides an interesting example of an initial density, which is nonsymmetric in the vertical direction. The limit mass distributions maintain a memory of such a density, demonstrating that mass transportation takes place locally, within a radius of order R, not globally.

This and the previous figures have been obtained using the infinity norm in the definition of the cut-off ξ, i.e., using $\xi_{\infty,R}$; results with the Euclidean norm, i.e., with $\xi_{2,R}$, are structurally similar for these cases, although the actual values of the positions and the strength of the deltas, as well as the critical values of R, may be different. Figure 9 documents the influence of the norm on the limit patterns; the upper part shows a substantial equivalence of the two patterns in the square case. The situation is completely different for the disk case, since the theory says (Corollary 10) that starting from a rotationally invariant initial measure, and using a rotationally invariant cut-off function such as $\xi_{2,R}$, the limit measure should be a single delta placed in the center of symmetry. Figure 7 is precisely obtained with $\xi_{2,R}$, yet more than one delta appears for sufficiently small R. This is clearly the effect of using meshes that are not rotationally invariant, so that the previous theoretical result cannot be reproduced at the discrete level. The lower part of Figure 9 indeed documents a significant difference

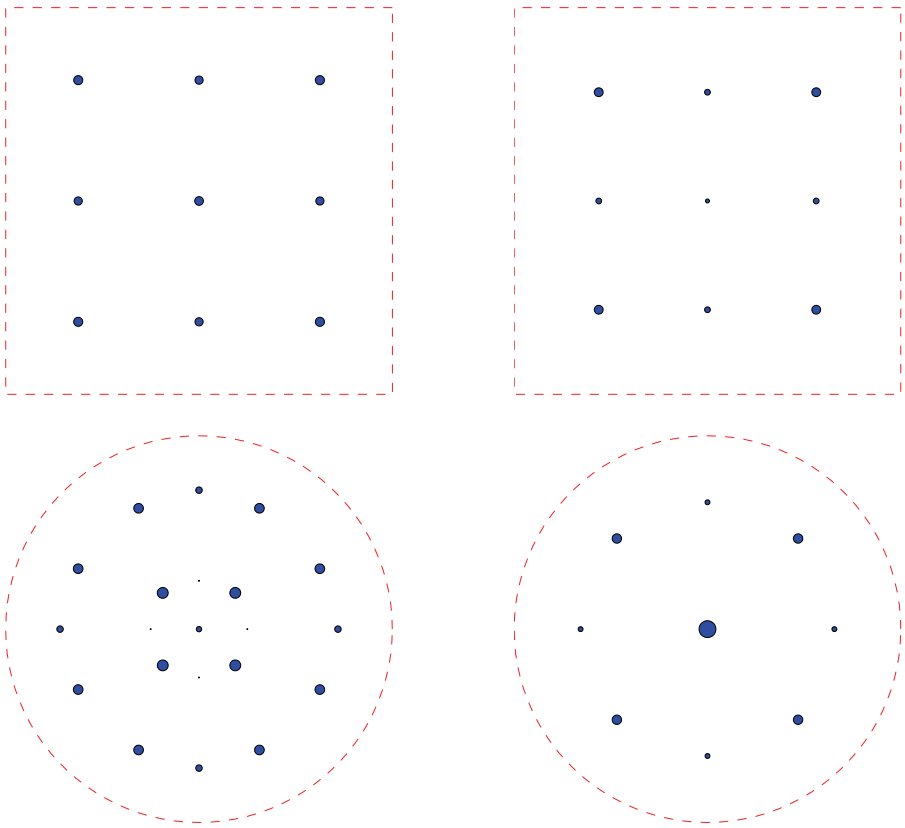

FIG. 9. *The influence of the distance $|x-y|$ used in the definition of the velocity V_t. Left-hand side plots are obtained by the Euclidean distance; right-hand side plots are obtained by the maximum norm distance. Squares: $R = 0.15$; disks: $R = 0.10$.*

between the two limit patterns. On the other hand, the lower right plot in Figure 7 seems to indicate that, if R is sufficiently small and the mesh is sufficiently fine, then the spurious deltas placed away from the center of symmetry become comparatively weaker than the central one.

REFERENCES

[1] L. AMBROSIO, N. GIGLI, AND G. SAVARÈ, *Gradient Flows in Metric Spaces and in the Space of Probability Measures*, Lectures Math. ETH Zurich, Birkhäuser Verlag, Basel, 2005.

[2] V.D. BLONDEL, J.M. HENDRICKX, AND J.N. TSITSIKLIS, *On Krause's consensus formation model with state-dependent connectivity*, IEEE Trans. Automat. Control, 54 (2009), pp. 2506–2517.

[3] V.D. BLONDEL, J.M. HENDRICKX, AND J.N. TSITSIKLIS, *Continuous-time average-preserving opinion dynamics with opinion-dependent communications*, SIAM J. Control Optim., 48 (2010), pp. 5214–5240.

[4] S. BOYD, A. GHOSH, B. PRABHAKAR, AND D. SHAH, *Randomized gossip algorithms*, IEEE Trans. Inform. Theory, 52 (2006), pp. 2508–2530.

[5] C. CANUTO, F. FAGNANI, AND P. TILLI, *A Eulerian approach to the analysis of rendez-vous algorithms*, in Proceedings of the 17th IFAC World Congress, Seoul, Korea, 2008, pp. 9039–9044.

[6] R. CARLI, F. FAGNANI, A. SPERANZON, AND S. ZAMPIERI, *Communication constraints in the average consensus problem*, Automatica, 44 (2008), pp. 671–684.

[7] J. Cortés, S. Martinez, and F. Bullo, *Robust rendezvous for mobile autonomous agents via proximity graphs in arbitrary dimensions*, IEEE Trans. Automat. Control, 51 (2006), pp. 1289–1298.
[8] F. Cucker and S. Smale, *Emergent behavior in flocks*, IEEE Trans. Automat. Control, 52 (2007), pp. 852–862.
[9] F. Cucker and S. Smale, *On the mathematics of emergence*, Japan J. Math., 2 (2007), pp. 197–227.
[10] F. Fagnani and S. Zampieri, *Randomized consensus algorithms over large scale networks*, IEEE J. Selected Areas of Communications, 26 (2008), pp. 634–649.
[11] A. Jadbabaie, J. Lin, and A. S. Morse, *Coordination of groups of mobile autonomous agents using nearest neighbor rules*, IEEE Trans. Automat. Control, 48 (2003), pp. 988–1001.
[12] U. Krause, *A discrete nonlinear and non-autonomous model of consensus formation*, in Communications in Difference Equations, S. Elaydi, G. Ladas, J. Popenda, and J. Rakowski, eds., Gordon and Breach, Amsterdam, 2000, pp. 227–236.
[13] R.J. LeVeque, *Finite Volume Methods for Hyperbolic Problems*, Cambridge University Press, New York, 2002.
[14] J. Lorenz, *A stabilization theorem for continuous opinion dynamics*, Phys. A, 355 (2005), pp. 217–223.
[15] J. Lorenz, *Continuous opinion dynamics of multidimensional allocation problems under bounded confidence. More dimensions lead to better chances for consensus Lorenz*, European J. Economic and Social Systems, 19 (2006), pp. 213–227.
[16] J. Lorenz, *Continuous opinion dynamics under bounded confidence: A survey*, Internat. J. Modern Phys. C, 18 (2007), pp. 1819–1838.
[17] L. Moreau, *Stability of multiagent systems with time-dependent communication links*, IEEE Trans. Automat. Control, 50 (2005), pp. 169–182.
[18] R. Olfati-Saber, J. A. Fax, and R. M. Murray, *Consensus and cooperation in networked multi-agent systems*, Proc. IEEE, 95 (2007), pp. 215–233.
[19] B. Piccoli and A. Tosin, *Pedestrian flows in bounded domains with obstacles*, Contin. Mech. Thermodyn., 21 (2009), pp. 85–107.
[20] B. Piccoli and A. Tosin, *Time-evolving measures and macroscopic modeling of pedestrian flow*, Arch. Rational Mech. Anal., 199 (2011), pp. 707–738.
[21] J. Tsitsiklis, *Problems in Decentralized Decision Making and Computation*, Ph.D. thesis, Department of Electrical Engineering and Computer Science, MIT, Cambridge, MA, 1984.